nature chemical biology

ARTICLES

Ever-fluctuating single enzyme molecules: Michaelis-Menten equation revisited

Brian P English[1], Wei Min[1], Antoine M van Oijen[1,4], Kang Taek Lee[1,4], Guobin Luo[1], Hongye Sun[1,4], Binny J Cherayil[1,2], S C Kou[3] & X Sunney Xie[1]

Enzymes are biological catalysts vital to life processes and have attracted century-long investigation. The classic Michaelis-Menten mechanism provides a highly satisfactory description of catalytic activities for large ensembles of enzyme molecules. Here we tested the Michaelis-Menten equation at the single-molecule level. We monitored long time traces of enzymatic turnovers for individual β-galactosidase molecules by detecting one fluorescent product at a time. A molecular memory phenomenon arises at high substrate concentrations, characterized by clusters of turnover events separated by periods of low activity. Such memory lasts for decades of timescales ranging from milliseconds to seconds owing to the presence of interconverting conformers with broadly distributed lifetimes. We proved that the Michaelis-Menten equation still holds even for a fluctuating single enzyme, but bears a different microscopic interpretation.

The quest to determine how enzymes work, essential to the understanding of life processes, continues to attract the fascination of enzymologists. Ever since the work of Michaelis and Menten[1], enzyme kinetics has had an essential role in the characterization of enzyme activities. The classic Michaelis-Menten equation provides a highly satisfactory description of enzymatic kinetics for large ensembles of enzyme molecules. However, recent advances in room-temperature single-molecule fluorescence studies[2–6] have allowed measurements of the distributions and fluctuations of molecular properties unattainable from ensemble data. Such measurements have shown that enzymes such as cholesterol oxidase[7], hairpin ribozyme[8], λ-exonuclease[9] and lipase[10,11] undergo temporal fluctuations of catalytic rates as a result of conformational fluctuations[12,13]. This finding has raised a number of intriguing questions. For example, how are single-molecule enzymatic measurements, which record stochastic waiting times of enzymatic reactions, reconciled with ensemble Michaelis-Menten kinetics? Why does the Michaelis-Menten equation work so well despite the broad distributions and dynamic fluctuations of single-molecule enzymatic rates? What new information is available from single-molecule experiments? In particular, what are the magnitude and timescales of the enzymatic rate fluctuations and what implication, if any, do these fluctuations have for cellular processes? Here we report a single-molecule assay of β-galactosidase that provides kinetic information over extended timescales (10^{-3}–10 s; 1–10^4 turnovers) and thereby allows us to address these questions.

According to the Michaelis-Menten mechanism, a substrate S binds reversibly with the enzyme E to form an enzyme-substrate complex ES. ES proceeds to product P, and E is regenerated for the next catalytic cycle.

$$E + S \underset{k_{-1}}{\overset{k_1}{\rightleftarrows}} ES \xrightarrow{k_2} E^0 + P, \qquad E^0 \xrightarrow{k_3} E \tag{1}$$

The Michaelis-Menten equation

$$v = \frac{v_{\max}[S]}{[S] + K_M} \tag{2}$$

gives explicitly the hyperbolic dependence of the enzyme velocity v on substrate concentration $[S]$ in an ensemble experiment, where $K_M = (k_{-1} + k_2)/k_1$ is the Michaelis constant, $[E]_T = [E] + [ES]$ is the total enzyme concentration and $v_{\max}$ is the maximum enzyme velocity. Under the condition of large k_3, as in the case discussed below, $v_{\max} = k_2[E]_T$. In a conventional Lineweaver-Burke plot, $1/v$ versus $1/[S]$ follows a linear relation[14].

Distinctly different from ensemble experiments, a single-molecule turnover experiment records the stochastic time trace of repetitive reactions of an individual enzyme molecule, from which the probability density of the waiting time τ for an enzymatic reaction to occur, $f(\tau)$, can be determined[7,15,16]. It has been shown that for the kinetic scheme in equation (1), $f(\tau)$ shows a single exponential rise, followed by a single exponential decay[15,17].

[1]Department of Chemistry and Chemical Biology, Harvard University, Cambridge, Massachusetts 02138, USA. [2]Department of Inorganic & Physical Chemistry, Indian Institute of Science, Bangalore 560012, India. [3]Department of Statistics, Harvard University, Cambridge, Massachusetts 02138, USA. [4]Present addresses: Department of Biological Chemistry and Molecular Pharmacology, Harvard Medical School, 240 Longwood Avenue, Boston, Massachusetts 02115, USA (A.M.v.O.); Department of Chemistry, University of Chicago, Chicago, Illinois 60637, USA (K.T.L.); Applied Biosystems, 850 Lincoln Center Dr., Foster City, California 94404, USA (H.S.). Correspondence should be addressed to X.S.X. (xie@chemistry.harvard.edu).

Received 15 November; accepted 29 November; published online 25 December 2005; doi:10.1038/nchembio759

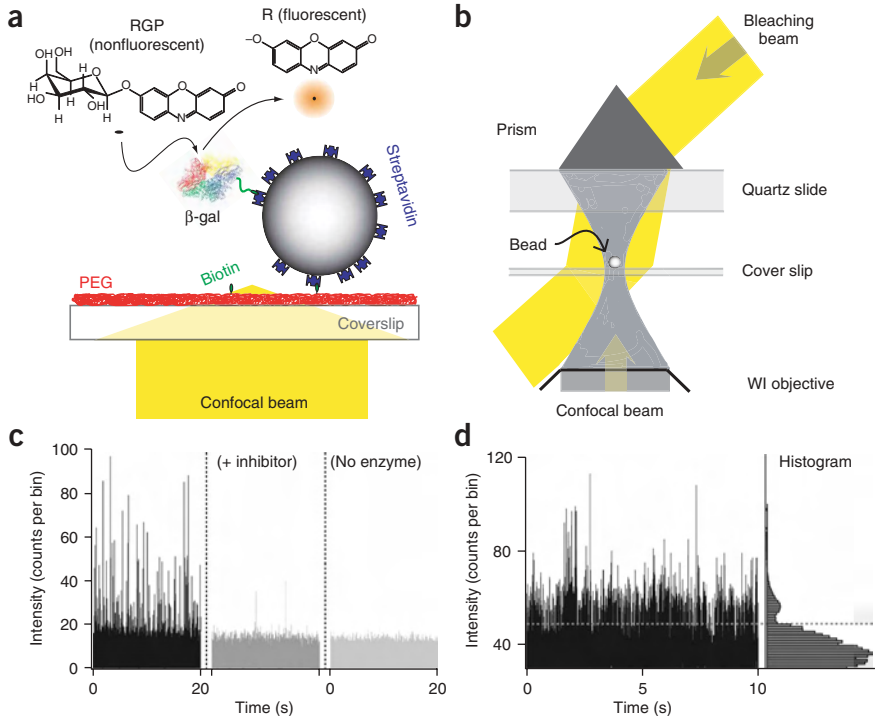

Figure 1 Single-molecule assay with fluorescent product. (**a**) Schematic representation of enzyme immobilization (not to scale). A single β-galactosidase molecule is linked to a streptavidin-coated polystyrene bead through a flexible PEG linker. The bead binds to the hydrophilic biotin-PEG surface of the glass coverslip. A photogenic resorufin-β-D-galactopyranoside (RGP, **1**) substrate in buffer solution is converted to a fluorescent resorufin (R, **2**) product by the single enzyme molecule, and detected one molecule at a time before it rapidly diffuses out of the confocal detection volume. (**b**) Schematic representation of the photobleaching and detection beams. A lens focuses a 550-mW, 560-nm photobleaching beam to a 200-μm-diameter spot surrounding the bead. The beam is coupled into the 100-μm-thick flow cell by a prism atop the quartz slide. The water immersion (WI) objective is used to focus a 1-mW, 560-nm detection beam onto a diffraction-limited spot around the bead and to collect the emission for detection with a photon-counting avalanche photodiode detector. (**c**) Turnover time trace of a single β-galactosidase molecule at 20 μM RGP. Left, fluorescence intensity as a function of time for a β-galactosidase molecule undergoing enzymatic turnovers, each giving a fluorescence burst. Middle, data for the same enzyme molecule after addition of 200 μM PETG inhibitor. Right, data for a bead without enzyme (no inhibitor). All time traces are obtained with 0.5-ms time bins. (**d**) Turnover time traces of a single β-galactosidase molecule at 100 μM RGP. Dashed line represents the threshold used to determine waiting times between two adjacent burst (see **Supplementary Methods** and **Supplementary Fig. 1** online). The intensity histogram of the enzymatic time trace is shown at right. The time trace has 0.5-ms time bins.

The concentration dependence of $f(\tau)$ is explicitly described in equation (3).

$$f(\tau) = \frac{k_1 k_2 [S]}{2A} [\exp(A+B)\tau - \exp(A-B)\tau] \quad (3)$$

where $A = \sqrt{(k_1[S] + k_{-1} + k_2)^2/4 - k_1 k_2 [S]}$ and

$B = -(k_1[S] + k_{-1} + k_2)/2$

The mean of τ is

$$\langle \tau \rangle = \int_0^\infty \tau f(\tau) d\tau$$

It follows from equation (3) that

$$\frac{1}{\langle \tau \rangle} = \frac{k_2 [S]}{[S] + K_M} \quad (4)$$

which is termed the single-molecule Michaelis-Menten equation[17].

Comparing equation (4) with equation (2), it is evident that the reciprocal of the mean waiting time measured in a single-molecule experiment is related to the enzymatic velocity measured in an ensemble experiment by $1/\langle \tau \rangle = \nu/[E]_T$. This relation originates from the equivalence between averaging over a single molecule's long time trace and averaging over a large ensemble of identical molecules. There are two types of ensemble enzymatic experiments[18]: one reports enzymatic velocities under steady-state conditions, which can be compared with $1/\langle \tau \rangle$; the other reports time-dependent population kinetics under pre–steady-state conditions, which can be compared with $f(\tau)$.

We set out to test experimentally the validity of equations (2) and (4), that is, the validity of the fundamental Michaelis-Menten equation at the single-molecule level. Single-molecule enzymatic assays involving fluorescence detection have previously been limited to short observation times because of photobleaching of fluorophores. To circumvent this problem, an assay with continuously replenished fluorescent product molecules was proposed[19] and then adapted for lipase[10,11]. In order to acquire the statistics necessary for reliable data analyses, we conducted experiments on β-galactosidase with a fluorogenic substrate that allowed us to extend observation lengths to $\sim 2 \times 10^4$ total turnovers. The analysis of these time traces not only confirmed the validity of the single-molecule Michaelis-Menten equation but also revealed a memory effect that lasts for decades of timescales. The characterization of such a memory effect, hidden in ensemble experiments, has provided new insights into how enzymes work on a single-molecule level.

RESULTS

Single-molecule assay with fluorescent product

Escherichia coli β-galactosidase is a 465-kDa enzyme that catalyzes the hydrolysis of lactose. The enzyme's crystal structural and biochemical details have been described[20,21]. Containing four catalytic sites, β-galactosidase is active only as tetramer[22]. It is known to obey the Michaelis-Menten equation[23,24], suggesting that the four well-separated catalytic sites are independent of each other[25]. In our investigations, instead of lactose, we used fluorogenic resorufin-β-D-galactopyranoside (RGP, **1**) (Molecular Probes) as the substrate[26]. Upon hydrolysis this molecule generates resorufin (R, **2**) as a fluorescent product (**Fig. 1a**). Using a fluorescence microscope, we continuously monitored enzymatic turnovers of a single immobilized β-galactosidase molecule immersed in a buffer solution of a constant substrate concentration. Each turnover was characterized by a

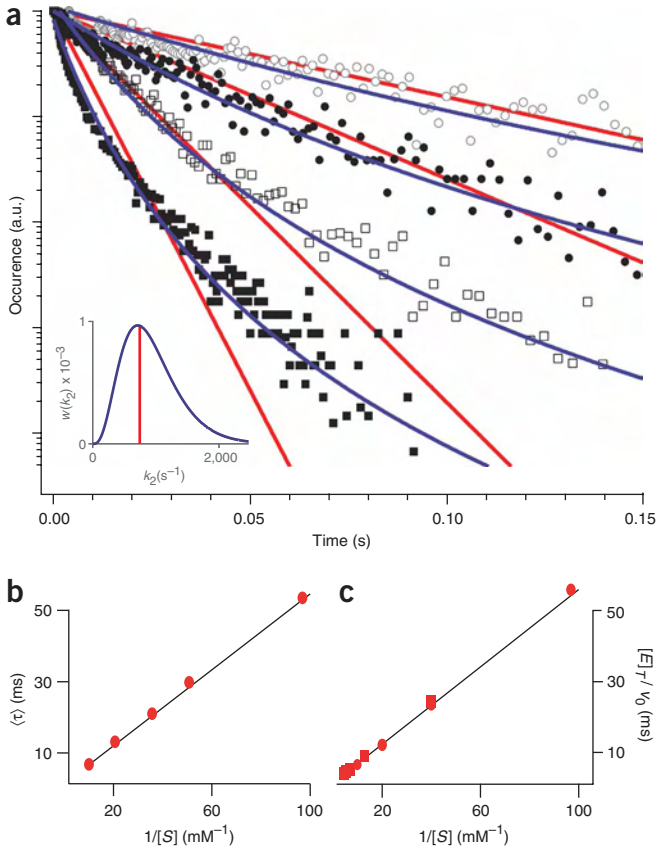

Figure 2 Concentration dependence of waiting time. (**a**) Histograms of the waiting time between two adjacent turnovers in a log-linear scale obtained from time traces of individual β-galactosidase molecules at four RGP concentrations, 10 μM (○), 20 μM (●), 50 μM (□) and 100 μM (■). The histograms change from monoexponential to multiexponential with increasing concentrations. Shown in blue are best global fits at all concentrations to $f(\tau)$ in the presence of dynamic disorder (equation (5)). We assume k_2 follows a gamma distribution, $w(k_2) = 1/\{b^a\Gamma(a)\}k_2^{a-1}\exp(-k_2/b)$, with $\Gamma(a)$ being the gamma function and a and b being the only adjustable parameters. The fitting parameters are $a = 4.2$ and $b = 220\ s^{-1}$, with $k_1 = 5 \times 10^7\ M^{-1}s^{-1}$ and $k_{-1} = 18{,}300\ s^{-1}$ (constrained by equation (8) with χ_2 and C_M obtained from **b**). The distribution (blue) and mean (red) of k_2 are shown in the inset. In contrast, shown in red are poor global fits of $f(\tau)$ in the absence of dynamic disorder (equation (3)) with the fitting parameter $k_2 = 730\ s^{-1}$, using the above k_1 and k_{-1}). (**b**) Single-molecule Lineweaver-Burke plot, $\langle\tau\rangle$ versus $1/[S]$ (red circles). Each data point is derived from one β-galactosidase molecule at the corresponding concentration. The black line depicts the fit with the single-molecule Michaelis-Menten equation (equation (6)), with $\chi_2 = 730 \pm 80\ s^{-1}$ and $C_M = 390 \pm 60$ μM. (**c**) Ensemble Lineweaver-Burke plot obtained at 11 pM (squares) and 53 pM (circles) biotin-β-galactosidase concentrations. The black line depicts the fit with the conventional Michaelis-Menten equation, equation (2), giving $v_{max}/[E]_T = 740 \pm 60\ s^{-1}$ and $K_M = 380 \pm 40$ μM, which are consistent with the χ_2 and C_M values, respectively, in **b**.

fluorescence burst from a resorufin molecule before it quickly diffused away from the probe volume of a tight laser focus (**Fig. 1b**). The residence times in the diffraction-limited confocal volume were less than the bin time of 500 μs. The burst intensities (**Fig. 1c,d**) vary because of different diffusion trajectories of the resorufin molecules out of the probe volume. Because resorufin is continuously produced by each turnover, observations could be made over long periods, limited only by the dissociation time of the β-galactosidase tetramer (several hours; see Methods and **Supplementary Fig. 2**).

We tethered single β-galactosidase molecules to polymer beads 490 nm in diameter, which were dispersed at an extremely low surface density onto a polymer-coated glass coverslip (**Fig. 1a**). This allowed us to locate enzyme molecules rapidly through difference interference contrast (DIC) images of the beads. The stoichiometry of bead-enzyme coupling (20:1) made it statistically unlikely that a bead would contain more than one β-galactosidase molecule. Special care was taken to avoid perturbation of the enzymatic activity by immobilization. The β-galactosidase molecules were biotinylated to the streptavidin-coated polystyrene beads via a flexible cysteine-reactive polyethylene glycol (PEG) linker. (As an important control, we measured the enzymatic velocities before and after coupling to the beads in an ensemble experiment with a fluorometer and found them to be the same, proving that enzyme activity is unperturbed by the beads; see **Supplementary Fig. 3**.) The beads then bound to the biotin-PEG surface of the coverslip, which has little affinity for both enzyme[27] and resorufin.

There existed a strong background signal caused by resorufin molecules that are continuously generated by autohydrolysis even in the absence of the enzyme (**Supplementary Fig. 4**) and that diffuse into the probe volume. In addition, resorufin molecules generated from previous or nearby enzymatic conversions can enter the probe volume. To circumvent this complication, we illuminated the area around the enzyme molecule with an intense laser beam (1,600 W cm^{-2}) (**Fig. 1b**) to bleach resorufin molecules diffusing into the probe volume, thus suppressing the background signal by at least two orders of magnitude (see **Supplementary Fig. 5**). However, a resorufin molecule generated by catalysis would not be photobleached during its short residence time within the probe volume.

Fluorescence-intensity time traces of enzymatic turnovers at 20 and 100 μM substrate concentrations at 22 °C are shown (**Fig. 1c,d**). As a control, we demonstrated that the signal disappeared when a competitive inhibitor, phenylethyl-β-D-thiogalactopyranoside (PETG), was introduced (**Fig. 1c**). As another control, we showed that no signal was visible when no β-galactosidase was bound to a bead (**Fig. 1c** and **Supplementary Methods** online for control experiments).

Michaelis-Menten equation with dynamic disorder

Plotting on a log-linear scale the waiting time between two adjacent fluorescence bursts obtained at substrate concentrations ranging from 10 to 100 μM RGP showed that at low substrate concentrations, the waiting-time histograms were monoexponential, as expected (see equation (3)) (**Fig. 2a**). At higher substrate concentrations, however, the waiting-time distributions became multiexponential, in disagreement with the prediction of monoexponential $f(\tau)$ (equation (3)) (compare the red curves of **Fig. 2a**). We note that the long tail in the multiexponential $f(\tau)$ is otherwise difficult to observe without a broad dynamic range and good statistics ($>3{,}000$ turnovers).

We attribute the multiexponential behavior of $f(\tau)$ to dynamic disorder[7,28,29], which refers to the fluctuations in the rate constants and is associated with conformational dynamics. It is well known that conformational changes, often triggered by substrate binding[30] and enzymatic reactions[31] within one catalytic cycle, are essential to enzyme functions. Nonetheless, it has long been inferred from ensemble-averaged experiments that a protein molecule undergoes conformational fluctuations on multiple timescales owing to rugged energy landscapes[32,33]. Fluctuations in single ion channels have been attributed to conformational changes[34]. Recently, such spontaneous

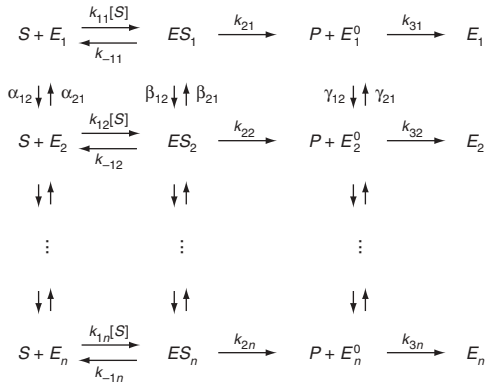

Scheme 1 Kinetic scheme of the multistate model involving n interconverting conformers. The multistate model is an extension of equation (1) where E, ES and E^0 are allowed to exist in any number n of mutually interconverting conformers. In this scheme, E_i not only interconverts with E_{i+1} and E_{i-1} but does so with all other conformers as well. This kinetic scheme does not include 'sequential' conformational intermediates induced by substrate binding or the enzymatic reaction within each catalytic cycle because their contributions to the long time fluctuation are less profound than those of the 'parallel' conformers.

conformational fluctuations have been directly observed and characterized at the single-molecule level on the timescale of 10^{-4}–10 s[12,13], a timescale longer than catalytic cycles. Although the microscopic characteristics of the conformers are yet unknown, they might be associated with the dynamic network of hydrogen bonds and electrostatic or ionic interactions within the protein. Mutation[35] and isotope[36] studies have indicated that either global or local conformational changes can affect enzymatic activity. Our premise is that the interconverting conformers possess different enzymatic reactivities. Therefore, the Michaelis-Menten mechanism can be represented by a kinetic scheme involving any number of interconverting conformers (**Scheme 1**).

Qualitatively, the concentration dependence of the multiexponential behavior of $f(\tau)$ can be understood as follows: at low substrate concentration, enzyme-substrate binding is rate limiting with a pseudo–first order rate constant, and hence $f(\tau)$ is a monoexponential decay. Indeed, the monoexponentiality of $f(\tau)$ at low $[S]$ argues for the lack of a broad distribution of k_{1i}. However, at high substrate concentrations, k_{2i} becomes rate-limiting, and the slow interconversion among the conformers ES_i results in a multiexponential decay of $f(\tau)$.

Quantitatively, when dynamic disorder is present only in k_2, that is when $k_{11} = k_{12} = \ldots = k_{1n} \equiv k_1$ (justified above) and $k_{-11} = k_{-12} = \ldots = k_{-1n} \equiv k_{-1}$ (to be justified later), and when interconversion among the ES_i conformers is slow compared to the enzymatic reaction, that is $\beta_{ij}/k_{2i} \rightarrow 0$, and α_{ij}/k_2 being small but nonzero (the quasi-static condition), $f(\tau)$ is the weighted average of k_{2i} conformers. Qualitatively, the quasi-static condition implies that the interconversion between the conformers is slow compared to the turnover time. We assume that k_2 has a continuous distribution, $w(k_2)$.

Under the condition of large number (n) of slowly interconverting conformers with different k_2 in a single enzyme molecule, it follows that

$$f(\tau) = \int_0^\infty dk_2 w(k_2) \frac{k_1 k_2 [S]}{2A} [\exp(A+B)t - \exp(B-A)t] \qquad (5)$$

where $w(k_2)$ denotes the probability density of k_2 for the conformers (see ref. 17). A and B are identical to the corresponding parameters in equation (3) for each conformer.

The observed histograms at all concentrations can be well fit globally to the predicted $f(\tau)$ assuming $w(k_2)$ is a gamma distribution using a maximum likelihood fitting procedure with $k_1 = 5 \times 10^7$ $M^{-1}s^{-1}$ and $k_{-1} = 18{,}300$ s^{-1} (**Fig. 2a**; blue curves). The resulting k_2 distribution (inset, **Fig. 2a**) highlights the extremely broad distribution of k_2, indicating the large number of conformers in a single enzyme molecule. Consistent with these findings, our Monte Carlo simulations have shown that the presence of even ten discrete conformers is not consistent with our experimental observations (see **Supplementary Methods** and **Supplementary Fig. 6**).

Notably, the reciprocal of the mean waiting time, $1/\langle\tau\rangle$, has been shown theoretically to obey a single-molecule Michaelis-Menten equation[17] under the quasi-static condition of dynamic disorder, a condition less stringent than the ones leading to equation (4).

$$\frac{1}{\langle\tau\rangle} = \frac{\chi_2 [S]}{[S] + C_M} \qquad (6)$$

Seemingly identical to the classic Michaelis-Menten equation (equation (2)), the hyperbolic concentration dependence is preserved even in the presence of dynamic disorder. However, unlike their counterparts $v_{max}/[E]_T$ and K_M, the parameters χ_2 and C_M carry distinctly different microscopic interpretations. Specifically,

$$\chi_2 = \frac{1}{\int_0^\infty \frac{w(k_2)}{k_2} dk_2} \qquad (7)$$

thus χ_2 is the weighted harmonic mean of k_2 for all conformers. Parallel with $K_M = (k_2 + k_{-1})/k_1$, the apparent Michaelis constant C_M is given by

$$C_M = (\chi_2 + k_{-1})/k_1 \qquad (8)$$

Hence χ_2 is dependent not only on the mean but also on the distribution of k_2. In other words, two mutations of an enzyme with an identical mean k_2 but different widths of the k_2 distributions would have different χ_2.

To verify the hyperbolic concentration dependence of the single-molecule Michaelis-Menten equation (equation (6)), we show a single-molecule Lineweaver-Burke plot, $\langle\tau\rangle$ versus $1/[S]$ (**Fig. 2b**), and compare it with the ensemble Lineweaver-Burke plot of

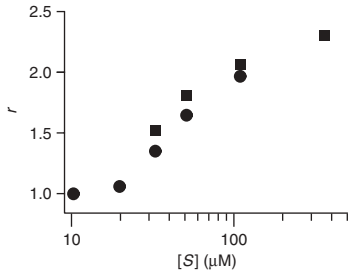

Figure 3 Concentration dependence of randomness parameter. Randomness parameter r as a function of substrate concentration. Circles, r obtained from waiting times of individual time traces: $r_\tau = (\langle\tau^2\rangle - \langle\tau\rangle^2)/\langle\tau\rangle^2$. Squares, r obtained from individual intensity time traces: $r_I = (\langle I^2\rangle - \langle I\rangle^2)/\langle I\rangle$ (see ref. 37, (equation (17)), consistent with r_τ at low concentrations, and obtainable even at the highest concentration (380 μM) when individual turnovers cannot be clearly resolved. That r is higher than unity at high substrate concentrations reveals the existence of dynamic disorder in k_2 but not in k_{-1}.

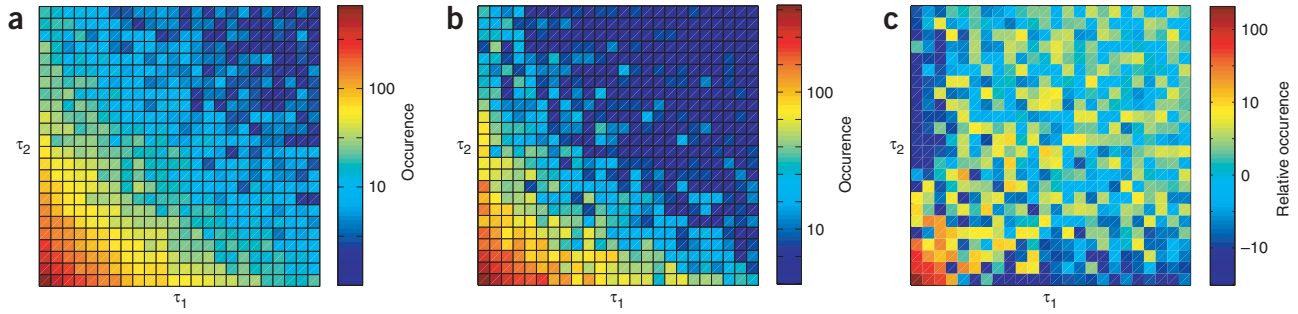

Figure 4 Two-dimensional joint-probability distributions of waiting times. (**a**) The 2D joint probability distribution of two adjacent waiting times (τ_1 and τ_2), $g(\tau_1,\tau_2)$, obtained from the time trace of a single β-galactosidase molecule at 100 μM substrate concentration. The τ_1 and τ_2 axes run from 0 to 12 ms. The color code represents the occurrence (*z* axis) from 500 (deep red) to 1 (dark blue). (**b**) The 2D joint probability distribution of two waiting times (τ_1 and τ_2) at a larger separation for same time trace as in **a**, which can be represented by $f(\tau_1)f(\tau_2)$ because of the lack of correlation between τ_1 and τ_2. The time axes are the same as in **a**. (**c**) The difference 2D histogram, $\delta(\tau_1, \tau_2) = g(\tau_1, \tau_2) - f(\tau_1)\, f(\tau_2)$. The time axes are the same as in **a**. The pixels in 'cold' colors (less probable) gather along two wings in the *x*-*y* plot, whereas those with 'warm' color (more probable) are mainly spread around the diagonal. A long waiting time tends to be followed by a long one, and a short waiting time tends to be followed by a short one.

biotin–β-galactosidase in solution (**Fig. 2c**). The least-squares fit in the former gives $\chi_2 = 730 \pm 80\ s^{-1}$ and $C_M = 390 \pm 60$ μM. The latter gives $v_{max}/E_T = 740 \pm 60\ s^{-1}$ and $K_M = 380 \pm 40$ μM (see **Supplementary Methods** online), which are consistent with the literature values for non-biotinylated enzymes[23,24,26]. The excellent agreement between χ_2 and v_{max}/E_T and between C_M and K_M, respectively, establishes the equivalence between $1/\langle\tau\rangle$ and the ensemble enzymatic velocity, and explains why the Michaelis-Menten equation is so widely applicable, even in the case of a multiexponential $f(\tau)$.

As a consistency check, under the condition that $w(k_2)$ is a gamma distribution with *a* and *b* values obtained from **Figure 2a**, equation (7) gives $\chi_2 = (a-1)b = 715\ s^{-1}$, which is consistent with the experimental χ_2 determined independently from the single-molecule and conventional Michaelis-Menten equations, respectively, as shown above.

Beyond just the consistency of the first moment of $f(\tau)$, $\langle\tau\rangle$, with ensemble measurements, the higher moments of $f(\tau)$ contain additional information. In particular, the second moment is related to the randomness parameter[37,38], $r = \{\langle\tau^2\rangle - \langle\tau\rangle^2\}/\langle\tau\rangle^2$. In the absence of dynamic disorder, *r* is unity at low or high substrate concentrations when there is only one rate-limiting step in equation (1), and less than unity at intermediate concentrations. We have shown theoretically that *r* becomes greater than unity for high concentrations in the presence of dynamic disorder in k_2 (ref. 17). Experimental measurement of *r* as a function of the substrate concentration (**Fig. 3**) showed that at low concentrations, *r* equals unity, as expected. Then parameter *r* rises above unity, however, as the dynamic disorder in k_2 becomes more apparent at increasing concentrations. We note that if the dynamic disorder were in k_{-1} instead of k_2, *r* would not be larger than unity[17], which corroborates the attribution of dispersed kinetics to dynamic disorder in k_2.

Memory effects of a single enzyme molecule

Besides the first and second moments of τ, a turnover time trace contains valuable information regarding temporal correlations between turnovers, which are inaccessible in ensemble data. To explore these correlations, we evaluate the two-dimensional (2D) joint probability $g(\tau_1, \tau_2)$ for two waiting times, τ_1 and τ_2, separated by a certain number of turnovers. Much discussed recently[39–43], this type of analysis was first introduced in analyzing time traces of cholesterol oxidase[7], for which only limited statistics were available. With much better statistics afforded by the long time traces in our experiment, we compared the 2D joint histogram for waiting times, τ_1 and τ_2, of two adjacent turnovers in a single-molecule time trace at 100 μM RGP concentration (**Fig. 4a**) with the 2D joint histogram of the same molecule for two turnovers with a large separation (**Fig. 4b**), which is described by $h(\tau_1, \tau_2) \equiv f(\tau_1)\, f(\tau_2)$ because of the loss of correlation. Were there no dynamic disorder, $g(\tau_1, \tau_2)$ and $h(\tau_1, \tau_2)$ would be the same. That these two histograms are different indicates the existence of a memory effect resulting from slow interconversion among the conformers. To highlight the memory effect, the difference histogram, $\delta(\tau_1, \tau_2) \equiv g(\tau_1, \tau_2) - h(\tau_1, \tau_2)$, is shown (**Fig. 4c**); this indicates that a short waiting time is less likely to be followed by a long waiting time, and vice versa.

Being a scrambled histogram, the difference histogram (**Fig. 4c**) does not explicitly reveal the timescales associated with the memory effect—that is, the fluctuation of the enzymatic velocity $k(t)$, defined as the number of turnovers per unit time. To extract this formation, we calculated the intensity autocorrelation function $C_I(t) = \langle\Delta I(0)\Delta I(t)\rangle/\langle\Delta I^2\rangle$, which characterizes the timescales of $k(t)$ fluctuations. With increasing substrate concentrations (**Fig. 5a**), $C_I(t)$ becomes more multiexponential as the dynamic disorder of k_2 is more apparent. As a control, we found that $C_I(t)$ is zero (**Fig. 5a**, in gray) when no enzyme molecule is in the probe volume. It should be noted that for $t > 0$, $C_I(t) = \langle\Delta I(0)\Delta I(t)\rangle/\langle\Delta I^2\rangle$ has no contribution from uncorrelated counting and background noise (see **Supplementary Methods** online).

However, $C_I(t)$ does not solely probe $k(t)$ fluctuations because it has a contribution from fluorophore diffusion[44], especially at low substrate concentrations (**Fig. 5a**, in red). To overcome this potential complication, we obtain the autocorrelation function of the waiting times

$$C_\tau(m) = \frac{\langle\Delta\tau(0)\Delta\tau(m)\rangle}{\langle\Delta\tau^2\rangle} \qquad (9)$$

as a function of m, the index number of turnovers and $\Delta\tau(m) \equiv \tau(m) - \langle\tau\rangle$. In the absence of dynamic disorder, $C_\tau(m) = 0$ for $m > 0$. The index number *m* is transformed to real time by $t = m\langle\tau\rangle$. It has been shown that $C_\tau(t)$ is approximately the normalized autocorrelation function of $k(t)$, $\langle\delta k(0)\delta k(t)\rangle/\langle\delta k^2\rangle$, under the limit of slow fluctuations of $k(t)$[45]. The blue trace in **Figure 5b** depicts $C_\tau(t)$ for the time trace with 100 μM RGP, which shows a decay similar to that of the $C_I(t)$ in **Figure 5a** (blue), only with a reduced time resolution (see **Supplementary Fig. 7** for a high time resolution). This

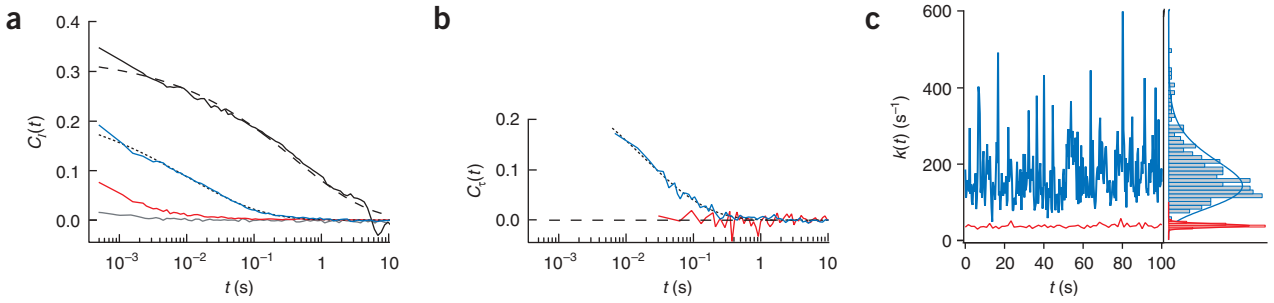

Figure 5 Fluctuations of turnover rate constants. (**a**) Intensity autocorrelation functions obtained from individual time traces of single β-galactosidase molecules at 20 μM (red), 100 μM (blue) and 380 μM (black) RGP. The intensity autocorrelation obtained 1 μm away from the enzyme is flat (in gray). At 100 μM, the dotted curve depicts the best fit to a stretched exponential: $C_I(t) = C_I(0)\ \exp[-(t/t_0)^\beta]$, with $\beta \sim 0.46$ and $t_0 \sim 0.017$ s. At 380 μM, the dashed curve depicts the best fit with $\beta \sim 0.4$ (more stretched) and $t_0 \sim 0.4$ s. We observed similar $C_I(t)$ for each of 23 individual enzyme molecules at 380 μM RGP ($\beta \sim 0.4 \pm 0.1$ and $t_0 \sim 0.4 \pm 0.1$ s). This $C_I(t)$ indicates that k_2 fluctuates at timescales spanning at least four decades (10^{-3}–10 s). (**b**) Waiting time autocorrelation functions, $C_\tau(t)$, obtained at 20 μM (red) and 100 μM (blue) RGP. The dotted curve depicts the best stretched exponential fit for **b** with parameters of $\beta = 0.45$ and $t_0 \sim 0.018$ s, identical to those for $C_I(t)$ at 100 μM. (**c**) Two time traces of the enzymatic velocities $k(t)$ of two single enzyme molecules at 20 μM (red) and 100 μM (blue) RGP concentration, respectively. Each data point is the average of 50 turnovers. The k histograms of the two time traces are shown on the right. The histograms are fit using gamma distributions as in **Figure 2a**, with $a = 71.5$ and $b = 0.5\ s^{-1}$ for the 20 μM, and with $a = 6.4$ and $b = 26.6\ s^{-1}$ for 100 μM RGP. The large amplitude of k fluctuation for the latter is evident.

consistency indicates that $C_I(t)$ reflects $\langle \delta k(0)\delta k(t) \rangle / \langle \delta k^2 \rangle$ at high concentrations. Unfortunately, $C_\tau(t)$ is not obtainable at an even higher concentration (380 μM) at which individual turnovers cannot be resolved and we revert to $C_I(t)$.

At 380 μM RGP, $C_I(t)$ is highly multiexponential (**Fig. 5a**, in black) and can be phenomenologically fit to a stretched exponential function $C_I(t) = C_I(0)\ \exp[-(t/t_0)^\beta]$ with $\beta = 0.4 \pm 0.1$ and $t_0 = 0.4 \pm 0.1$ s. $C_I(t)$ is monoexponential when $\beta = 1$ and shows a long tail in the decay when $\beta < 1$. We observed a low β value ($\beta \sim 0.4$) for each of the 23 enzyme molecules examined at the same substrate concentration. This highlights the broad range of timescales of $k(t)$ fluctuations, spanning at least four decades from 10^{-3}–10 s. Notably, this coincides with the same timescales at which conformational fluctuations within a single protein molecule have been observed[12,13]. This strongly argues that enzymatic fluctuations do indeed originate from conformational fluctuations.

We determined the distribution of $k(t)$ by binning every 50 turnovers along the turnover time trace. The $k(t)$ distributions of two enzyme molecules at 100 and 20 μM RGP (**Fig. 5c**) show that, as expected, the distribution at 20 μM was narrow because substrate binding is rate limiting. At 100 μM, the overall profile of the k distribution is well fit by a gamma distribution, which corroborates the assumption of gamma distribution made earlier. The broad width of the gamma distribution indicates that dynamic disorder is by no means a small effect.

DISCUSSION

The very large amplitude and broad timescales of enzymatic rate fluctuations at the single-molecule level, which are uncovered by analyses of long turnover time traces, highlight the fact that an enzyme molecule is an ever-fluctuating dynamic entity during catalysis. Despite its apparent generality[7–11], this phenomenon has been hidden in the ensemble enzymatic assays for two reasons. First, in pre–steady-state ensemble measurements, data often lack the dynamic range necessary to identify long tails in multiexponential kinetics. Second, in steady-state ensemble measurements, data are masked by the fact that the Michaelis-Menten equation holds not only for the simplistic case of a single conformer but also more generally for the case of a large number of slowly interconverting conformers with different enzymatic activities.

The effects of enzymatic fluctuations would be less significant for a system comprising many enzyme molecules. However, if a system contains a small number of enzyme molecules, as is often the case in a living cell, the enzymatic fluctuations could be readily manifested. Biologically important as they might be, such fluctuations might now be probed on a single-molecule basis in living cells.

METHODS

Substrate purification. The photogenic substrate solution has to be free of even trace amounts of resorufin before single-molecule turnovers can be observed. Resorufin-β-D-galactopyranoside (RGP) (Molecular Probes) was always newly purified at the start of each experiment using an anion-exchange FPLC column (HiTrap Q XL, Amersham) after most resorufin was removed by acidic chloroform extraction. A low-ionic-strength, pH 7.5 buffer containing 10 mM triethanolamine was used to elute the substrate at a concentration of 0.6 mM. Unless otherwise noted, all ensemble and single-molecule experiments were conducted in 25 mM dibasic phosphate buffer (pH adjusted to 7.5) containing 0.25 M NaCl, 5 mM $MgCl_2$, 0.05 mg ml^{-1} BSA (New England Biolabs), 0.005% Tween-20 (Sigma) and 10% (w/w) PEG (8,000 MW, Sigma).

Estimation of tetramer dissociation. It is well known that β-galactosidase is inactivated at very dilute concentrations owing to dissociation of the tetrameric enzyme. To determine the timescale of tetramer dissociation, we recorded the enzymatic activity, as a function of time, of 2 pM of biotin-linked β-galactosidase immobilized on 1-μm-diameter streptavidin-coated beads present in excess. At various time points, the beads were separated from solution by centrifugation and the amount of active enzyme measured using a fluorometer (**Supplementary Fig. 3**) with 200 μM RGP. In this experiment, the low concentration of the immobilized enzyme assured that no recombination occurred after tetramer dissociation. The enzyme activity decayed exponentially (**Supplementary Fig. 2**), giving a time constant of tetramer dissociation of 5.6 ± 0.7 h, which defined a time window in which the experiment had to be completed.

Linking enzyme to functionalized-glass surface. Owing to the high catalytic efficiency of β-galactosidase, the presence of large amounts of enzyme in the flow cell would markedly increase the background level of resorufin fluorophores. To avoid this, the surface concentration of immobilized enzyme was maintained at roughly one enzyme molecule per square millimeter (for β-galactosidase functionalization and characterization, see **Supplementary**

Methods online). To make it possible to rapidly locate an enzyme molecule at such dilute concentrations, the enzyme was coupled to streptavidin-coated polystyrene beads (490-nm diameter, Bangs) that were large enough to be visualized by DIC microscopy. The streptavidin-coated beads were chosen because they contribute no fluorescence signal under laser excitation and have little affinity for resorufin.

Biotin-linked enzyme (10 nM) and beads were incubated for 1 h at 4 °C. Because the tetrameric enzyme dissociates at very low concentrations, the incubation was conducted in a ten-fold excess of non-biotinylated β-galactosidase. Immediately before the single-molecule experiment, the beads were separated from unbound enzyme by centrifugation. The bead-enzyme coupling reaction was controlled such that most beads were without enzyme (>95%). This made it statistically unlikely (<0.25%) that an active bead would carry more than one β-galactosidase enzyme.

Before the start of the bead incubation, the flow cell was flushed with 0.1 mg ml^{-1} BSA and 0.01% Tween-20 to inhibit nonspecific binding of beads to the tubing and to the surfaces of the flow cell (see **Supplementary Methods** online for preparation of the flow chamber). The streptavidin beads bound specifically to the biotinylated PEG surface of the coverslip. The surface density of the beads was monitored through the eyepiece by DIC microscopy and the beads in solution were flushed out when a low surface density of several beads per 100 μm^2 was obtained.

Optical detection. An argon-ion laser (Innova 308, Coherent) provided 5 W of multiline power that was used to pump a rhodamine 110 dye laser (Model 599, Coherent). The dye laser was tuned to 560 nm and was filtered using a Z560/10-nm excitation filter (Chroma). The dye laser produced stable output power of 600 mW. A wedge was used to split the beam into a weak confocal beam and a strong bleaching beam (550 mW). An acousto-optical modulator (AOM 40, IntraAction) was used to stabilize the confocal beam to 1 mW. In combination with a Nikon TE 300 inverted microscope and a Nikon 60x water-immersion objective, a single-photon avalanche detector (SPAD, Perkin-Elmer SPCM-AQR-14) was used to detect fluorescence signals. A long-pass dichroic (568 nm cutoff) and two emission filters (LP 580, E 610/55, both from Chroma) separated resorufin fluorescence from excitation light. A telescope (×4 magnification) was used to match the diameter of the detected beam to the chip size of the SPAD, which was used as the confocal pinhole.

The more powerful bleaching beam continuously irradiated a large area around the immobilized enzyme. The bleaching beam was coupled into the flow cell by a prism on top of the quartz slide that was immersed in a thin layer of immersion oil (type FF, Cargille Laboratories) and was focused to a spot 200 μm in diameter. The bleaching angle was optimized so that the bleaching beam did not enter the objective to keep Raman and scattering background levels low (**Fig. 1b**).

***In situ* photobleaching.** To detect fluorescence from resorufin molecules generated by enzymatic reactions, we used a strong photobleaching beam to eliminate unwanted fluorescence signals from resorufin molecules arising from the following three processes: (i) both ion-exchange FPLC and reverse-phase HPLC chromatography leave residual resorufin at the nanomolar level; (ii) the RGP substrate has a low but measurable autohydrolysis rate (**Supplementary Fig. 4**); (iii) resorufin molecules from turnovers of neighboring immobilized β-galactosidase molecules enter the probe volume.

A strong and defocused laser beam illuminated and continuously photobleached the area within a 100-μm radius of the immobilized enzyme, which reduced the unwanted fluorescent signal by at least two orders of magnitude (**Supplementary Fig. 5**). The excitation intensity of the bleaching beam was high enough so that unwanted resorufin molecules were bleached before they diffused into the detection volume. Resorufin molecules created only within the diffraction-limited confocal volume were detected before photobleaching.

To assure efficient bleaching, all experiments were conducted in PEG (8,000 MW, Sigma) to prolong the residence time of a resorufin molecule (see **Supplementary Methods** online).

Note: Supplementary information is available on the Nature Chemical Biology website.

ACKNOWLEDGMENTS

We thank E.J. Sánchez for developing the scanning software and P. Blainey for his help with Matlab simulations. This work was funded by a US National Institutes of Health (NIH) R01 grant and recently by the NIH Director's Pioneer Award to X.S.X. B.P.E. is supported by an NIH Training Grant. K.T.L is supported by the Post-doctoral Fellowship Program of Korea Science & Engineering Foundation. A.M.v.O. acknowledges financial support from the Niels Stensen Foundation. S.C.K. acknowledges support from an NSF grant and an NSF CAREER award.

COMPETING INTERESTS STATEMENT

The authors declare that they have no competing financial interests.

Published online at http://www.nature.com/naturechemicalbiology/
Reprints and permissions information is available online at http://npg.nature.com/reprintsandpermissions/

1. Michaelis, L. & Menten, M.L. Kinetics of invertase action. *Biochem. Z.* **49**, 333–369 (1913).
2. Moerner, W.E. & Orrit, M. Illuminating single molecules in condensed matter. *Science* **283**, 1670–1676 (1999).
3. Xie, X.S. & Trautman, J.K. Optical studies of single molecules at room temperature. *Annu. Rev. Phys. Chem.* **49**, 441–480 (1998).
4. Ishijima, A. & Yanagida, T. Single molecule nanobioscience. *Trends Biochem. Sci.* **26**, 438–444 (2001).
5. Weiss, S. Fluorescence spectroscopy of single biomolecules. *Science* **283**, 1676–1683 (1999).
6. Bustamante, C., Bryant, Z. & Smith, S.B. Ten years of tension: single-molecule DNA mechanics. *Nature* **421**, 423–427 (2003).
7. Lu, H.P., Xun, L. & Xie, X.S. Single-molecule enzymatic dynamics. *Science* **282**, 1877–1882 (1998).
8. Zhuang, X. *et al.* Correlating structural dynamics and function in single ribozyme molecules. *Science* **296**, 1473–1476 (2002).
9. van Oijen, A.M. *et al.* Single-molecule kinetics of λ exonuclease reveal base dependence and dynamic disorder. *Science* **301**, 1235–1239 (2003).
10. Velonia, K. *et al.* Single-enzyme kinetics of CALB-catalyzed hydrolysis. *Angew. Chem. Intl. Edn.* **44**, 560–564 (2005).
11. Flomenbom, O. *et al.* Stretched exponential decay and correlations in the catalytic activity of fluctuating single lipase molecules. *Proc. Natl. Acad. Sci. USA* **102**, 2368–2372 (2005).
12. Yang, H. *et al.* Protein conformational dynamics probed by single-molecule electron transfer. *Science* **302**, 262–266 (2003).
13. Min, W., Luo, G., Cherayil, B.J., Kou, S.C. & Xie, X.S. Observation of a power-law memory kernel for fluctuations within a single protein molecule. *Phys. Rev. Lett.* **94**, 198302/1–198302/4 (2005).
14. Segel, I.H. *Enzyme Kinetics: Behavior and Analysis of Rapid Equilibrium and Steady State Enzyme Systems* (Wiley, New York, 1993).
15. Xie, X.S. Single-molecule approach to enzymology. *Single Molecules* **2**, 229–236 (2001).
16. Qian, H. & Elson, E.L. Single-molecule enzymology: stochastic Michaelis-Menten kinetics. *Biophys. Chem.* **101–102**, 565–576 (2002).
17. Kou, S.C., Cherayil, B.J., Min, W., English, B.P. & Xie, S.X. Single-molecule Michaelis-Menten equations. *J. Phys. Chem. B* **109**, 19068–19081 (2005).
18. Fersht, A. *Structure and Mechanism in Protein Science: A Guide to Enzyme Catalysis and Protein Folding* (Freeman, New York, 1999).
19. Edman, L., Foldes-Papp, Z., Wennmalm, S. & Rigler, R. The fluctuating enzyme: a single molecule approach. *Chem. Phys.* **247**, 11–22 (1999).
20. Jacobson, R.H., Zhang, X.J., DuBose, R.F. & Matthews, B.W. Three-dimensional structure of β-galactosidase from *E. coli*. *Nature* **369**, 761–766 (1994).
21. Richard, J.P., Huber, R.E., Heo, C., Amyes, T.L. & Lin, S. Structure-reactivity relationships for β-galactosidase (*Escherichia coli*, lacZ). 4. Mechanism for reaction of nucleophiles with the galactosyl-enzyme intermediates of E461G and E461Q β-galactosidases. *Biochemistry* **35**, 12387–12401 (1996).
22. Marchesi, S.L., Steers, E., Jr. & Shifrin, S. Purification and characterization of the multiple forms of β-galactosidase of *Escherichia coli*. *Biochim. Biophys. Acta* **181**, 20–34 (1969).
23. Seong, G.H., Heo, J. & Crooks, R.M. Measurement of enzyme kinetics using a continuous-flow microfluidic system. *Anal. Chem.* **75**, 3161–3167 (2003).
24. Hadd, A.G., Raymond, D.E., Halliwell, J.W., Jacobson, S.C. & Ramsey, J.M. Microchip device for performing enzyme assays. *Anal. Chem.* **69**, 3407–3412 (1997).
25. Matthews, B.W. The structure of *E. coli* β-galactosidase. *C. R. Biol.* **328**, 549–556 (2005).
26. Hofmann, J. & Sernetz, M. Immobilized enzyme kinetics analyzed by flow-through microfluorimetry. Resorufin-β-D-galactopyranoside as a new fluorogenic substrate for β-galactosidase. *Anal. Chim. Acta* **163**, 67–72 (1984).
27. Ha, T. *et al.* Initiation and re-initiation of DNA unwinding by the *Escherichia coli* Rep helicase. *Nature* **419**, 638–641 (2002).
28. Zwanzig, R. Rate processes with dynamical disorder. *Acc. Chem. Res.* **23**, 148–152 (1990).

29. Karplus, M. Aspects of protein reaction dynamics: deviations from simple behavior. *J. Phys. Chem. B* **104**, 11–27 (2000).
30. Mesecar, A.D., Stoddard, B.L. & Koshland, D.E., Jr. Orbital steering in the catalytic power of enzymes: small structural changes with large catalytic consequences. *Science* **277**, 202–206 (1997).
31. Hammes, G.G. Multiple conformational changes in enzyme catalysis. *Biochemistry* **41**, 8221–8228 (2002).
32. Austin, R.H., Beeson, K.W., Eisenstein, L., Frauenfelder, H. & Gunsalus, I.C. Dynamics of ligand binding to myoglobin. *Biochemistry* **14**, 5355–5373 (1975).
33. Frauenfelder, H., Sligar, S.G. & Wolynes, P.G. The energy landscapes and motions of proteins. *Science* **254**, 1598–1603 (1991).
34. Sakmann, B. & Neher, E. *Single-Channel Recording* 2nd edn. (Plenum, New York and London, 1995).
35. Benkovic Stephen, J. & Hammes-Schiffer, S. A perspective on enzyme catalysis. *Science* **301**, 1196–1202 (2003).
36. Kohen, A., Cannio, R., Bartolucci, S. & Klinman, J.P. Enzyme dynamics and hydrogen tunnelling in a thermophilic alcohol dehydrogenase. *Nature* **399**, 496–499 (1999).
37. Schnitzer, M.J. & Block, S.M. Statistical kinetics of processive enzymes. *Cold Spring Harb. Symp. Quant. Biol.* **60**, 793–802 (1995).
38. Svoboda, K., Mitra, P.P. & Block, S.M. Fluctuation analysis of motor protein movement and single enzyme kinetics. *Proc. Natl. Acad. Sci. USA* **91**, 11782–11786 (1994).
39. Yang, S. & Cao, J. Two-event echos in single-molecule kinetics: a signature of conformational fluctuations. *J. Phys. Chem. B* **105**, 6536–6549 (2001).
40. Lippitz, M., Kulzer, F. & Orrit, M. Statistical evaluation of single nano-object fluorescence. *ChemPhysChem* **6**, 770–789 (2005).
41. Lerch, H.-P., Rigler, R. & Mikhailov, A.S. Functional conformational motions in the turnover cycle of cholesterol oxidase. *Proc. Natl. Acad. Sci. USA* **102**, 10807–10812 (2005).
42. Flomenbom, O., Klafter, J. & Szabo, A. What can one learn from two-state single-molecule trajectories? *Biophys. J.* **88**, 3780–3783 (2005).
43. Barsegov, V., Chernyak, V. & Mukamel, S. Multitime correlation functions for single molecule kinetics with fluctuating bottlenecks. *J. Chem. Phys.* **116**, 4240–4251 (2002).
44. Magde, D., Elson, E. & Webb, W.W. Thermodynamic fluctations in a reacting system. Measurement by fluorescence correlation spectroscopy. *Phys. Rev. Lett.* **29**, 705–708 (1972).
45. Yang, S. & Cao, J. Direct measurements of memory effects in single-molecule kinetics. *J. Chem. Phys.* **117**, 10996–11009 (2002).

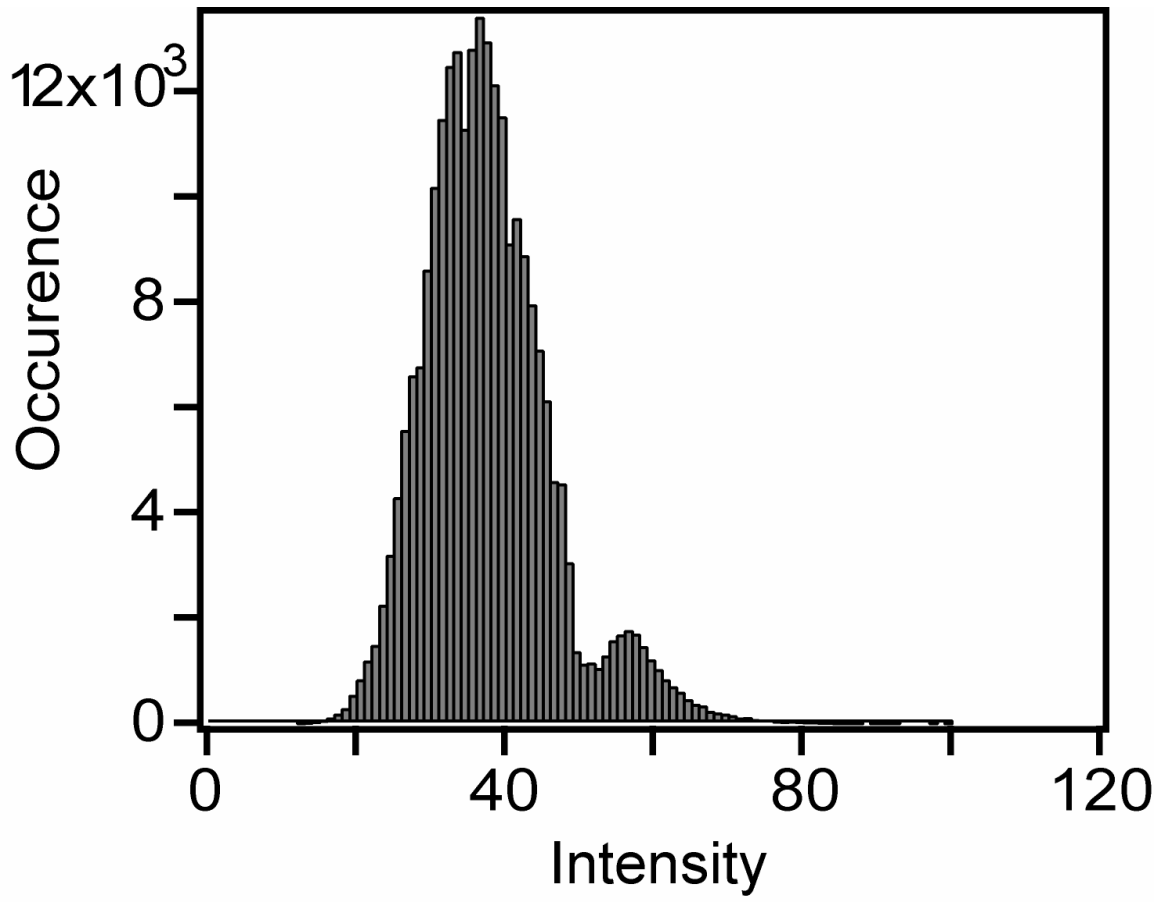

Supplementary Figure 1 Intensity histogram.

Histogram for an intensity time trace at 100 μM RGP. The histogram is composed of a background distribution and a signal distribution, each fitted with a Poisson distribution. The intersection at the two fitted Poisson distributions yields the threshold, above which a fluorescent spike is considered to be an enzymatic turnover.

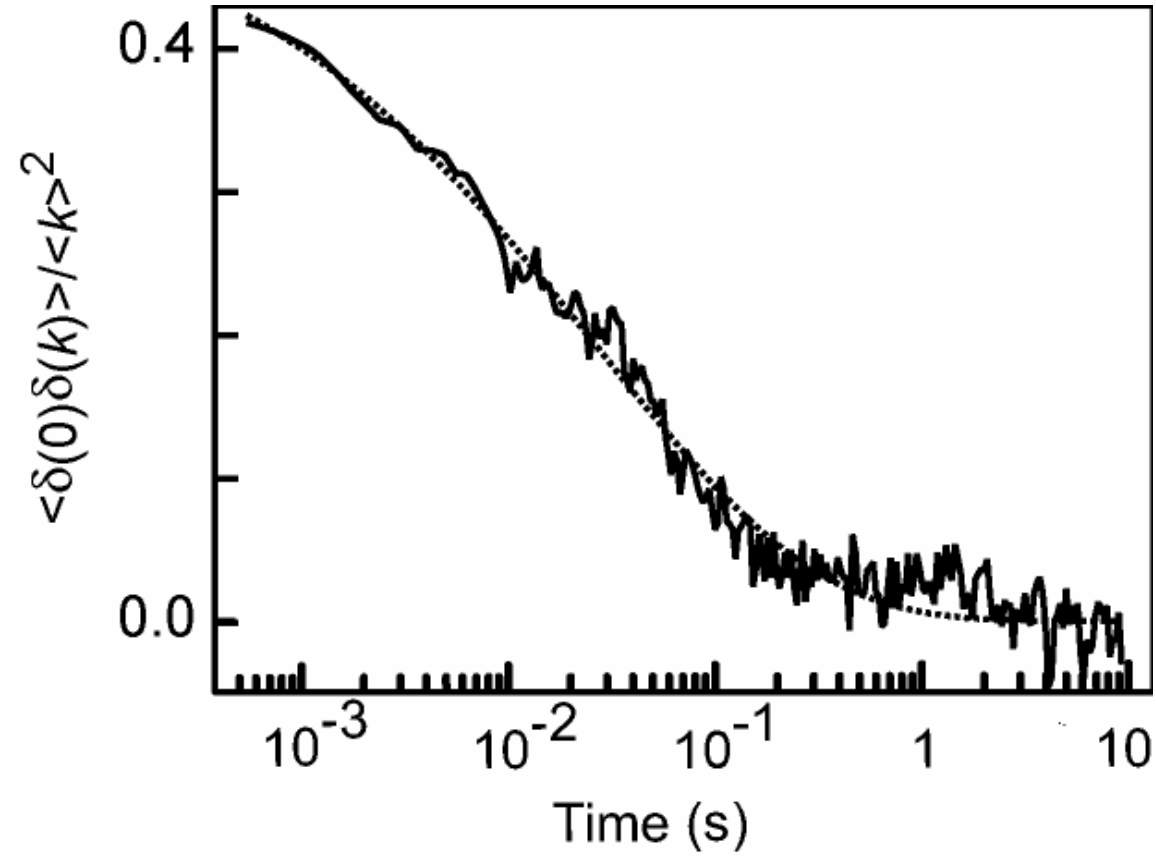

Supplementary Figure 7 Autocorrelation of *k*(*t*).

k(*t*), $\langle \delta k(0)\delta k(t) \rangle / < k >^2$, obtained from a single enzyme molecule at 100 μM RGP concentration. The dotted curve depicts the best to a stretched exponential decay, $k(\mathrm{t}) = \mathrm{k}(0)\exp[-(t/t_o)^{\beta}]$, with β = 0.43 and t_0 ~ 20 ms. The broad range of time scales of *k* fluctuation is evident.

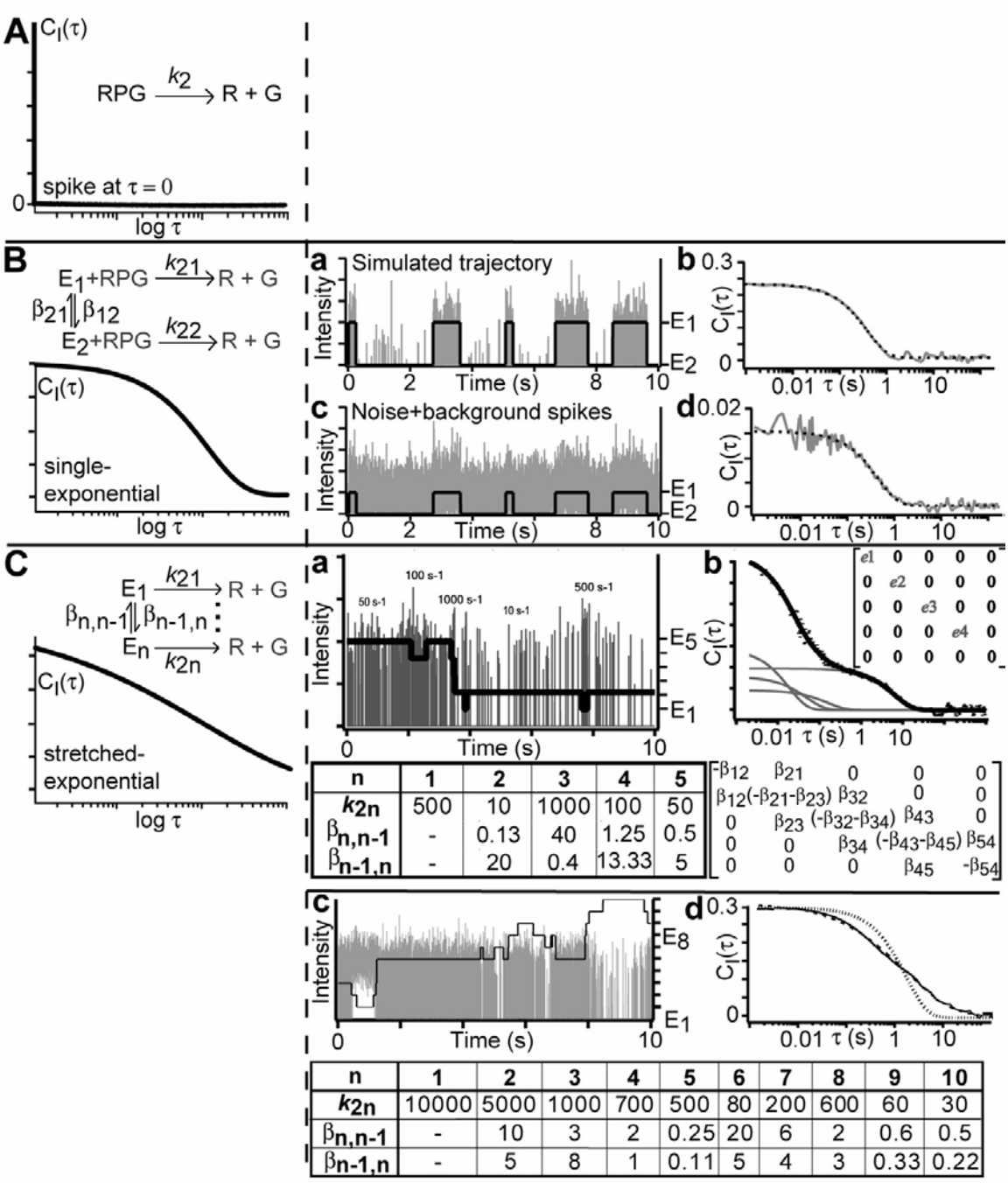

n	1	2	3	4	5
k_{2n}	500	10	1000	100	50
$\beta_{n,n-1}$	-	0.13	40	1.25	0.5
$\beta_{n-1,n}$	-	20	0.4	13.33	5

$$\begin{matrix} -\beta_{12} & \beta_{21} & 0 & 0 & 0 \\ \beta_{12} & (-\beta_{21}-\beta_{23}) & \beta_{32} & 0 & 0 \\ 0 & \beta_{23} & (-\beta_{32}-\beta_{34}) & \beta_{43} & 0 \\ 0 & 0 & \beta_{34} & (-\beta_{43}-\beta_{45}) & \beta_{54} \\ 0 & 0 & 0 & \beta_{45} & -\beta_{54} \end{matrix}$$

n	1	2	3	4	5	6	7	8	9	10
k_{2n}	10000	5000	1000	700	500	80	200	600	60	30
$\beta_{n,n-1}$	-	10	3	2	0.25	20	6	2	0.6	0.5
$\beta_{n-1,n}$	-	5	8	1	0.11	5	4	3	0.33	0.22

Supplementary Figure 6 Monte-Carlo simulations

Simulations of intensity autocorrelation functions defined as $C_I(\tau) = \frac{<\delta I(t)\delta I(t+\tau)>}{<\delta I^2>}$.

(**A**) $C_I(\tau)$ is a spike at τ = 0 for a constant catalytic rate (k_2).

(**B**) $C_I(\tau)$ is a single exponential if an enzyme has two conformers with catalytic rate constants k_{21} and k_{22}. If the interconversion rates are β_{12} and β_{21}, one observes an autocorrelation curve that decays single-exponentially with a rate constant equal to the sum of β_{12} and β_{21}.
The autocorrelation analysis is insensitive to both the counting noise and also to the signal of the background noise (single molecules diffusing through the probe volume). This is illustrated by two simulated time traces:

(**a**) A turnover time trace with two conformational states (k_{21} = 1000 s^{-1} and k_{22} = 10 s^{-1}) is simulated with interconversion rates β_{12} and β_{21} that are
2 s^{-1} and 0.5 s^{-1}, respectively. The switching between the two conformers is indicated by the solid black line overlaid with the time trace.
(**b**) $C_I(\tau)$ of this simulated time trace decays exponentially with a rate constant of 2.5 s^{-1} (see dotted curve).
(**c**) Both background noise mimicking molecules diffusing through the probe volume at high rates (1000 s^{-1}) and also counting noise are added to the time traces in **a**.
(**d**) Insensitive to counting and background noise for t > 0, $C_I(\tau)$ decays single exponentially with a decay constant of 2.5 s^{-1}.

(**C**) $C_I(\tau)$ for multiple interconverting conformers.

(**a**) Simulation of five interconverting conformers with the kinetic rate matrix depicted.
(**b**) $C_I(\tau)$ of **a** is the sum of the four single exponentials (*e*1 to *e*4, in gray).
(**c**) Simulation of ten interconverting conformers with the kinetic rate matrix depicted.
(**d**) $C_I(\tau)$ of **c** with the best stretched-exponential fit (β = 0.5) (dashed curve) and single-exponential fit (dotted curve).

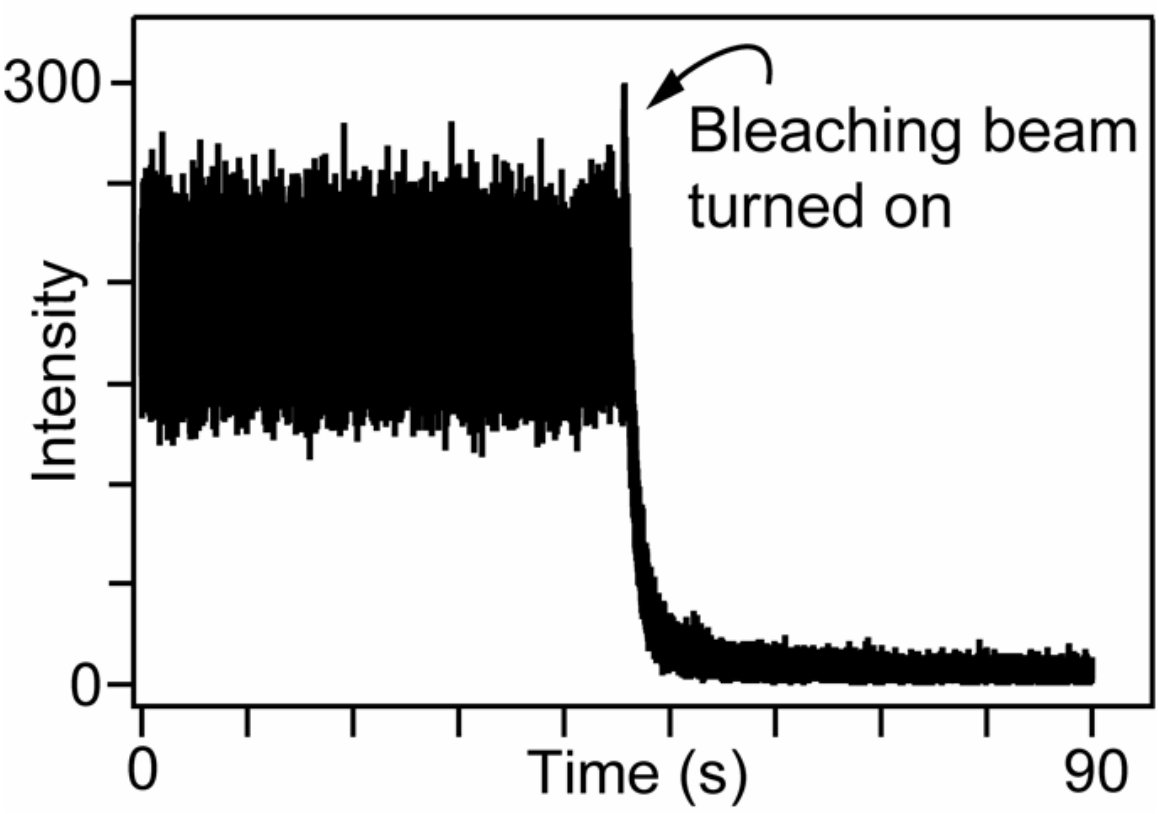

Supplementary Figure 5 Effectiveness of the bleaching scheme.

Confocal detection of 0.1 mM RGP in 15 % PEG solution. Before the bleaching beam is turned on, residual resorufin impurities give rise to high fluorescence intensities. When the bleaching beam is turned on, the unwanted signal is reduced by at least two orders of magnitude.

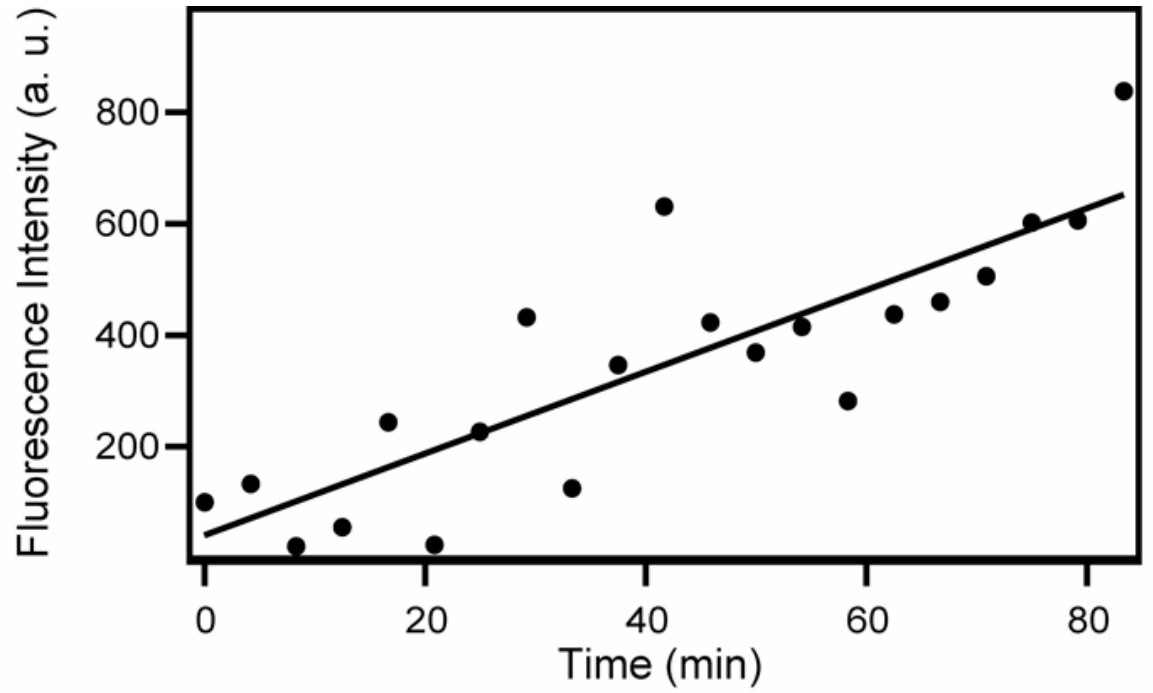

Supplementary Figure 4 Autohydrolysis rate.

Measurement of RGP autohydrolysis rate at 10 μM RGP. At the experimental pH = 7.5, the fluorescence signal increases linearly due to resorufin generated by autohydrolysis. The slope corresponds to an autohydrolysis rate of 0.14 ± 0.02 $\mu M_R\ M_{RGP}^{-1}\ min^{-1}$.

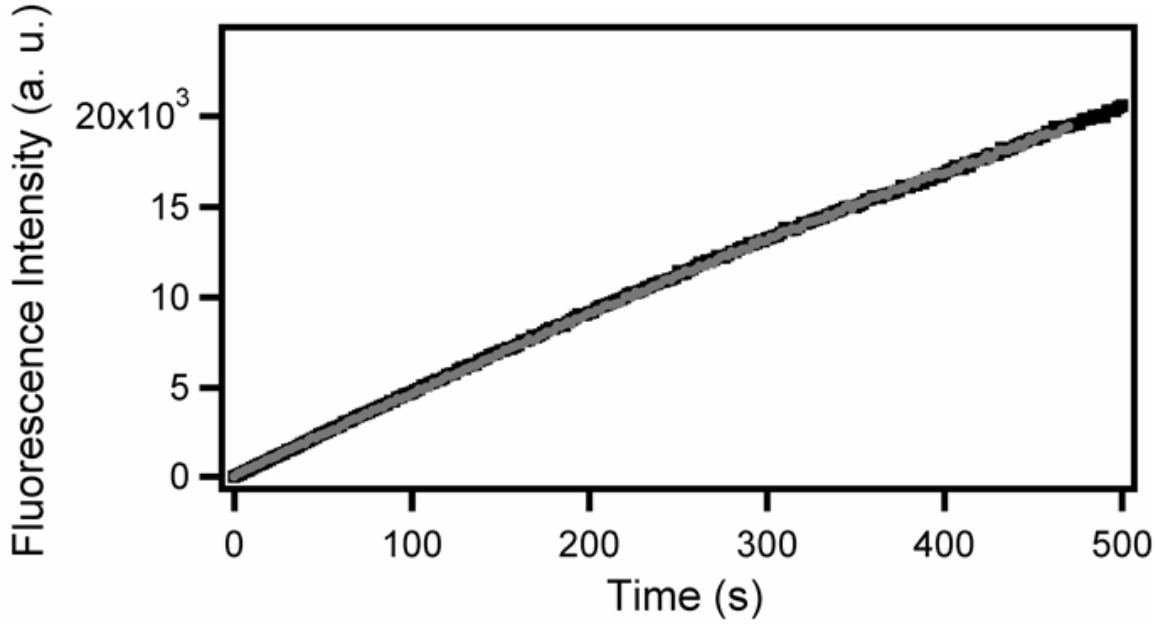

Supplementary Figure 3 Effect of surface immobilization on enzymatic activity.

Ensemble measurements of enzymatic activity of biotin-β-galactosidase free in solution and immobilized to streptavidin beads, taken with a fluorometer. Black squares: Fluorescence increase upon addition of 10 pM biotin-PEG-functionalized enzyme into the solution of 10 μM RGP. Gray circles: Fluorescence increase upon addition of 10 pM of biotin-functionalized enzyme coupled streptavidin beads in excess. The fact that enzymatic reactivity of the beta-galactosidase remains unchanged proves that enzymatic activity is not perturbed by surface-immobilization.

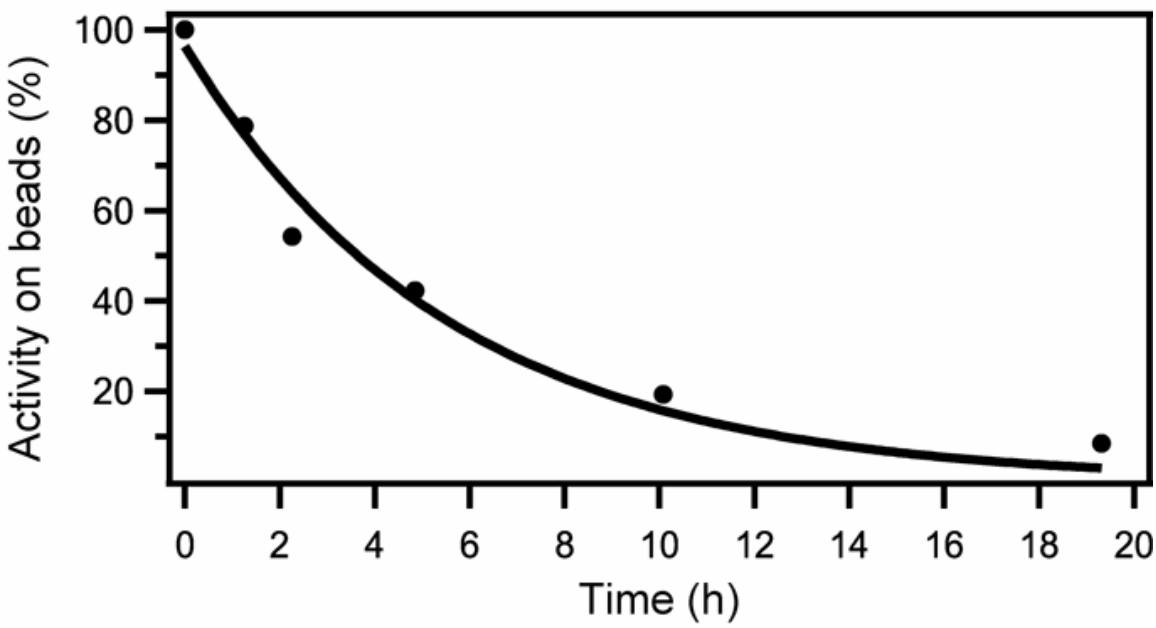

Supplementary Figure 2 Loss of enzymatic activity due to tetramer dissociation.

The enzymatic activity is measured for 20 pM of β-galactosidase linked to streptavidin beads with 1:100 stoichiometry ratio, as in **Supplementary Fig. 3**. The exponential decay yields a time constant of 5.6 ± 0.7 hr for tetramer dissociation.

Supplementary Methods

Enzyme functionalization and characterization

E. *coli* β-galactosidase (Grade VIII, Sigma) is purified using a Zorbax GF-250 size-exclusion HPLC column (Agilent) in pH 7 phosphate (dibasic) buffer containing 10 mM $MgCl_2$ and 145 mM NaCl. The enzyme is concentrated using a 10K centrifuge filter (Centricon) at 4˚C to a concentration of 3μM and is then coupled to a 4 kDa biotin-PEG-maleimide linker (Nektar Pharmaceutical). The maleimide moiety of the linker can react specifically with a surface-accessible cysteine. Incubation with 4 μM of the bi-functional linker is conducted at room temperature for three hours. The reaction is quenched using 10 mM β-mercaptoethanol (Sigma). The aliquoted enzyme is stored in 50% glycerol buffer at –80 ˚C.

Large streptavidin-coated polystyrene beads (1 μm diameter, Bangs) allow for easy separation of biotin-linked enzyme from unlinked enzyme and were used to determine how many reactive PEG-biotin linkers are coupled to an enzyme molecule. After a short incubation of an aliquot of enzyme with an excess of beads, all biotin-functionalized β-galactosidase will be linked to the beads and hence biotin-functionalized enzyme can easily be separated from solution via centrifugation. Using a fluorometer, the ratio of biotinylated to non-biotinylated enzyme was determined by comparing the enzymatic activity on the beads to the activity of non biotin-functionalized enzyme remaining in solution. Both activities were measured in buffer containing 200 μM RGP. The ratio of biotinylated to non-biotinylated enzyme was determined to be 1:3. Hence it is unlikely that one tetrameric enzyme has more than one biotin-linkers. We conclude that only one of the subunits is tethered to a bead.

We observed that the enzymatic rate of the enzyme before and after immobilization to the surface of the beads are the same, which proves that the enzyme is unperturbed after being linked to the surface with the long and flexible PEG linker (see **Supplementary Fig. 3**).

Flow chamber

A flow cell is prepared by carving out a 7 mm wide channel in 100 μM thick adhesive spacer (Grace Bio Labs) that is sandwiched between a functionalized coverslip and a quartz microscope slide. The quartz microscope slide has two holes that accommodate polyethylene tubing used for easy buffer exchange. The silanization reagent 3-aminopropyltriethoxysilane (Sigma) is used to amine-functionalize coverslips that have been thoroughly cleaned using alternating rounds of sonication in ethanol and 1M sodium hydroxide. After a 5 min incubation at pH = 8.2, the silanization reagent is cured onto the slip at 120 °C for 30 min. The amine-functionalized coverslips are then incubated with amine-reactive PEG and amine-reactive biotin-PEG at a ratio of 100:1 (both from Nektar) for 3 hours. The layer of PEG makes the coverslip more hydrophilic and hence prevents unspecific hydrophobic surface interactions. The biotinylated coverslips are stored under vacuum until use.

Intensity thresholding

To differentiate product fluorescence spikes from background noise, we first construct the intensity histogram of the time trace, as shown in **Supplementary Figure 1**. The histogram is composed of two contributions: a background peak and a signal peak, each fitted well with a Poisson distribution. The intersection between the two fitted

Poisson distributions sets the threshold I^*, above which a fluorescence spike is considered to arise from a enzymatic turnover.

Determination of ensemble MM-coefficients

We determine initial enzymatic velocity as a function of RGP concentration by recording the increase in fluorescence using a fluorometer for two biotin-linked β-galactosidase concentrations: 11 pM and 53 pM. Newly purified RGP is diluted to concentrations of 10, 25, 50, 100, 200 and 250 μM (at 53 pM β-galactosidase), or 25, 75, 150, 200, 250 μM RGP concentration (at 11 pM β-galactosidase). Two Lineweaver-Burke plots are shown **Figure 2b** in the main text. The slope of a Lineweaver-Burke plot is $K_M / v_{\max}$, the *y*-intercept is $1/v_{\max}$ and the extrapolated x-intercept is $-1/K_M$. Values of K_M and $v_{\max}$ are derived from a global weighted least-squares fit of both curves and a $v_{\max}$ value of 740 ± 60 s^{-1} and a K_M value of 380 ± 40 μM is obtained.

Diffusion in poly(ethylene-glycol)

To assure efficient bleaching, all experiments are conducted in PEG (8000 MW, Sigma) to prolong the resident time of a resorufin molecule. Unlike glycerol, PEG acts as a macroviscogen, and increases the viscosity at large dimensions by forming pores within which the diffusion of small molecules is unaffected[1,2]. Hence PEG does not affect the Michaelis k_2 and K_M[3]. In ensemble experiments conducted on the fluorometer, we found increasing PEG up to 20 % (w/w) concentrations did not substantially affect enzymatic turnover rates. For all experiments conducted between 20 and 100 μM RGP, the final PEG concentration is adjusted to 10 % (w/w). For all experiments conducted at 380 μM, the PEG concentration is increased to 15 % (w/w).

Control experiments

An important control is to be able to turn off enzymatic activity of a single enzyme molecule. To do so, we used a competitive inhibitor phenylethyl-β-D-thiogalactopyranoside (PETG, Molecular Probes) and observed that enzymatic turnovers were halted (**see Fig. 1c** in main text). This proves that signal is solely due to enzymatic turnovers.

It is also important that the enzyme has to bind to the bead specifically through the biotinylated linker, rather than through nonspecific binding. In another control experiment, beads are incubated with non-biotinylated β-galactosidase at high concentrations, and we observe no beads exhibiting fluorescence signals (hence enzymatic activity).

Intensity autocorrelation analysis

Supplementary Figure 6 illustrates the autocorrelation functions of three hypothetical kinetic scenarios: an enzyme with only one constant turnover rate produces a flat intensity autocorrelation curve (**Supp. Fig. 6A**). If a single exponential decay is observed in the intensity autocorrelation curve, the enzyme must have two interconverting conformers with differing turnover rates. Its decay rate then reveals the sum of the two interconversion rates (**Supp. Fig. 6B**). More and more interconverting conformations will result in an autocorrelation function that is increasingly more multi-exponential (**Fig. S6C**).

Autocorrelation analysis has the advantage that it is insensitive to background noise and spikes due to fluorescent molecules diffusing through the probe volume. This is illustrated by a simulation in which both counting noise and background spikes are artificially added into the intensity time trace (**Supp. Fig. 6B**, right panel). For simplicity, the simulated enzymatic time trace has only two conformers. As expected, in the absence of noise, $C_I(t)$ is a single-exponential with a decay time-constant equal to the inverse sum of the two interconverting rate constants. With the addition of both background noise and diffusing molecules, there is a spike at t = 0 with an amplitude given by the variances of all sources of intensity fluctuations. For t > 0, the functional form of the autocorrelation curve is unaffected by the counting and background noise.

Monte-Carlo simulations of multiple conformers

The experimentally observed $C_I(t)$ at high substrate concentration can be phenomenologically fit well to a stretched-exponential function (β = 0.4) (see black trace in **Fig. 5a** in main text).

With five interchanging conformers, the autocorrelation curves $C_I(t)$ from time-traces obtained by Monte-Carlo simulations can never be fit well to a stretched-exponential function (**Supp. Fig. 6C** top panel). Only when the interconversion (0.13 s^{-1} to 10 s^{-1}) and turnover rates (10 s^{-1} to 1000 s^{-1}) are chosen to be broadly distributed can $C_I(t)$ be fit to a sum of four exponential decays corresponding to the four eigen-values of the rate-matrix ($e1$ to $e4$). The switching and turnover rates are tabulated.

With ten interchanging conformers, a reasonable fit to a stretched exponential $C_I(t)$ (β = 0.5) to the autocorrelation curve of the simulated time-trace can only be obtained with a small pre-selected set of interconverting (0.11 s^{-1} to 10 s^{-1}) and turnover rates (20 s^{-1} to 10000 s^{-1}) (**Supp. Fig. 6C** bottom panel). The switching and turnover rates are tabulated. However, the simulated time traces look distinctly different from the observed ones (**Fig 1d**, main text) as the simulated turnover time-traces under this condition are composed of prolonged segments of very high (10000 s^{-1}) and very low (30 s^{-1}) enzymatic activity.

These Monte-Carlo simulations demonstrate that a large number (rather than a few) of interconverting conformers are necessary to explain the highly stretched autocorrelation functions of turnover velocity observed experimentally.

Autocorrelation function of *k*

In addition to $C_\tau(t)$ discussed in the main text, we can obtain autocorrelation function $<\delta k(0)\delta k(t)>$ according to:

$$<\delta k(0)\delta k(t)> / <k>^2 = N(t) / <k> - 1$$

where $N(t)$ is the probability density function of any two turnover events separated by time t regardless of the number of turnovers in between[4]. In the absence of k fluctuation, $N(t)$ is a constant k, and $<\delta k(0)\delta k(t)>$ is zero for all times. **Supplementary Figure 7** depicts $<\delta k(0)\delta k(t)> / <k>^2$ for the time trace at 100 μM RGP concentration, which exhibits the same temporal decays of the corresponding $C_I(t)$ and $C_\tau(t)$, but without sacrificing temporal resolution as for $C_\tau(t)$. The consistency at 100 μM RGP indicates that at an even higher concentration, such as 380 μM, $C_I(t)$ must also reflect fluctuations in $k(t)$. At 380 μM RGP, $<\delta k(0)\delta k(t)>$ cannot be evaluated directly because individual turnovers cannot be resolved.

References

1. Biancheria, A. & Kegeles, G. J. Diffusion measurements in aqueous solutions of different viscosities. *J. Am. Chem. Soc.* **79**, 5908-5912 (1957).
2. Muhr, A. H. & Blanshard, J. M. Diffusion in gels. *Polymer* **23**, 1012-1026 (1982).
3. Bulychev, A. & Mobashery, S. Class C β-lactamases operate at the diffusion limit for turnover of their preferred cephalosporin substrates. *Antimicrob. Agents Chemother*. **43**, 1743-1746 (1999).
4. Yang, S. & Cao, J. Direct measurements of memory effects in single-molecule kinetics. *Journal of Chemical Physics* **117**, 10996-11009 (2002).

Ever-fluctuating single enzyme molecules: Michaelis-Menten equation revisited

Brian P English, Wei Min, Antoine M van Oijen, Kang Taek Lee, Guobin Luo, Hongye Sun, Binny J Cherayil, S C Kou & X Sunney Xie
Nat. Chem. Biol. **2**, 87–94 (2006)

In the print version of this article and the version initially published online, the subsection "Estimation of tetramer dissociation" of the Methods contained an error. The second sentence should read: "To determine the timescale of tetramer dissociation, we recorded the enzymatic activity, as a function of time, of 20 pM of biotin-linked β-galactosidase immobilized on 1-μm-diameter streptavidin-coated beads present in excess". The error has been corrected in the HTML and PDF versions of the article. This correction has been appended to the PDF version.